Autonomous Monitoring of Breathing Debonds in Bonded Composite Structures Using Nonlinear Ultrasonic Signals

SHIRSENDU SIKDAR

ABSTRACT

This study aims to develop a structural health monitoring model that autonomously assesses breathing-type debonds between the base plate and stiffener in lightweight composite structures. The approach utilizes a specifically designed deep learning architecture that employs nonlinear ultrasonic signals for automatic debond assessment. To achieve this, a series of laboratory experiments were conducted on multiple composite panels with and without base plate-stiffener debonds. A network of piezoelectric transducers (actuators/sensors) was used to collect time-domain guided wave signals from the composite structures. These signals, representing nonlinear signatures such as higher harmonics, were separated from the raw signals and transformed into time-frequency scalograms using continuous wavelet transforms. A convolutional neural network-based deep learning architecture was designed to extract discrete image features automatically, enabling the characterization of composite structures under healthy and variable breathing-debond conditions. The proposed deep learning-assisted health monitoring model exhibits promising potential for autonomous inspection with high accuracy in complex structures that experience breathing-debonds.

Cardiff School of Engineering, Cardiff University, The Parade, Queen's Building, Cardiff, CF24 3AA, UK
University of Huddersfield, Department of Engineering and Technology, School of Computing and Engineering, HD1 3DH, United Kingdom

INTRODUCTION

Lightweight composites have become increasingly popular in various engineering sectors, including aeronautics, aerospace, marine, infrastructure, and automobile, due to their advantageous properties such as high stiffness-to-weight ratio, fire resistance, and acoustic damping [1]. Bonded stiffened composites are commonly employed for

lightweight construction in these fields [2], where different types of stiffeners are bonded to the base plate of the structures. However, the bond between the stiffener and base plate can experience breathing-type debonding caused by cyclic loading, improper handling, impact, and aging [3]. If left undetected, these debonds can expand over time and result in catastrophic structural failures [4]. Therefore, the detection and characterization of these hidden damages in stiffened composites are of utmost importance.

Previous studies [5-6] have demonstrated the potential of structural health monitoring (SHM) methods based on guided wave (GW) propagation for accurate detection of concealed defects in complex composites with multiple layers. These SHM techniques, utilizing linear and nonlinear GW propagation, offer long-range monitoring with high sensitivity to minor defects or discontinuities in layers [7]. Typically, lightweight and cost-effective broadband transducers, such as a network of surface-mounted piezoelectric lead zirconium titanate transducers (PZTs), are used in these SHM methods [5-6].

Breathing debonds in composites pose a challenge for traditional SHM methods [8]. The breathing-type debond can exhibit open (debond) or closed (undamaged) behavior due to the occurrence of "breathing" under dynamic wave loading. The breathing phenomenon generates nonlinear ultrasonic waves with mixed frequency-response, nonlinear resonance, sub-harmonics, and higher harmonics [9]. The nonlinear response features are indicative of contact-type damage, such as breathing cracks or kissing-delaminations, and are less influenced by operational conditions [10]. The generation of higher harmonics, associated with contact nonlinearity often observed in breathing-type damage, has been analyzed by various researchers [11]. In [9], the occurrence of contact-acoustic non-linearity (CAN) due to breathing-type cracks was investigated using signals from a PZT network.

In recent years, machine learning approaches based on structural response data have gained popularity for autonomous condition monitoring of structures [12-13]. Deep learning algorithms, particularly Convolutional Neural Networks (CNN), have shown their effectiveness in image-based characterization of structural conditions [14]. CNN algorithms excel in handling grid-like inputs, such as images, and extract similar features from local regions with similar patterns [14]. Image-based deep learning involves large datasets that can be synthetically generated by adding different levels of noise (e.g., Gaussian zero mean noise) to actual images, a technique known as "data augmentation" [40-42]. Recent studies [12-14] have proposed deep learning-based SHM methods for autonomous assessment of static damage or delamination in laminated composites. However, there is a research gap in the identification of nonlinear ultrasonic wave features induced by breathing-type damage using an automated deep learning approach. This paper aims to address this gap by presenting a deep learning-based SHM strategy.

In this paper, a CNN-based structural health monitoring (SHM) strategy is proposed for automatically characterizing carbon fibre-reinforced stiffened composite panels

(SCPs) with and without baseplate-stiffener debonds. The strategy utilizes both the raw guided wave (GW) signals and the filtered time-domain higher-harmonic signals. The characterization is achieved through a series of laboratory experiments using multiple SCP samples. The GW signals obtained from the experimental approaches are transformed into RGB scalograms (representing time-frequency information) using the Continuous Wavelet Transform (CWT). These scalograms are then employed as input to the deep learning architecture specifically designed for this purpose, enabling training, validation, and testing operations.

LABORATORY EXPERIMENTS

The experiments involved a series of ultrasonic guided wave (GW) tests conducted on different healthy and baseplate-stiffener debonded samples of stiffened composite panels (SCPs).

In each SCP sample, two L-shaped stiffeners measuring 30 × 30 mm and having a length of 450 mm were attached to the baseplate, which had dimensions of 500 × 450 × 2 mm. Epoxy resin adhesive was used for bonding the stiffeners to the baseplate. To create artificial debonds at the stiffener-baseplate interface, 0.05 mm thin Teflon films measuring 30 × 30 mm were placed during the manufacturing process for samples (ii) and (iii). A network of bonded lead zirconium titanate (PZT) transducers, with a thickness of 0.05 mm and a diameter of 10 mm, was mounted on the top surface of the SCPs. These PZTs were responsible for generating and receiving ultrasonic signals. A signal generation and acquisition system with a sampling rate of 1M sample/s was used to control the PZTs (Figure 1). The SCP samples were constructed using quasi-isotropic laminates with lay-up (0/90/+45/-45)s made of carbon-fiber (CFCL) and had a thickness of 2 mm.

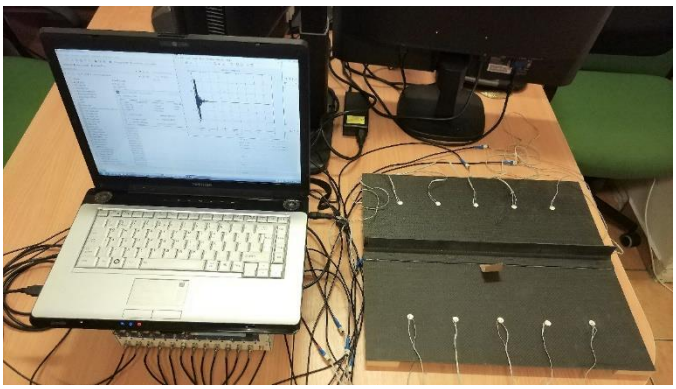

Figure 1. Laboratory-based experimental setup for PZT-induced GW propagation in the SCPs.

Figure 1 illustrates the setup used in the laboratory for the SCP sample with the DSt2 debond, which includes a PZT network comprising 10 sensors (S1, … S10) and an actuator labeled as 'A'. The excitation signal was determined through a series of trials involving various carrier frequencies and cycles. Among the tested signals, a 7-cycle tone-burst sine signal exhibited the most pronounced higher harmonics in the frequency domain. To identify a suitable actuation frequency, a series of 7-cycle sine waves with different carrier frequencies were applied through the actuator 'A', and the resulting signals were collected at sensor 'S3' (Figure 1). This process enabled the generation of

a frequency-response plot, depicted in Figure 2(a), which indicated higher response magnitudes around 150 kHz. Consequently, a Hanning window-modulated 7-cycle 150 kHz sine pulse, shown in Figure 2(b), was selected as the excitation signal for the experiments. In Figure 2(b), the Fast Fourier Transform (FFT) of the actuator signal in the frequency domain is presented. The actuator PZT introduces the excitation signal (Figure 2(a)) and initiates the propagation of guided waves within the SCP. These guided waves are detected by each of the PZT sensors (S1, S2, …, S10) within the network.

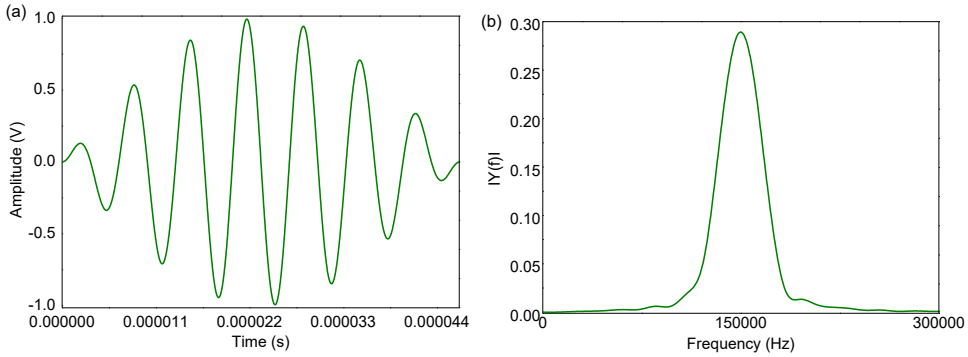

Figure 2. (a) Selected actuator excitation signal and (b) its FFT.

DEEP LEARNING BASED SHM STRATEGY

The proposed structural health monitoring (SHM) strategy utilizes the time-history signals of guided waves (GW) captured by the sensors. These signals are transformed into time-frequency scalogram images using Continuous Wavelet Transform (CWT) with the Morse Wavelet. CWT involves convolving the input dataset with a set of functions generated by the mother wavelet, and this convolution can be efficiently computed using an FFT algorithm. The output of CWT is a complex-valued function, except for the complex mother wavelet, which ensures that the CWT is a real-valued function along the positive real axis. Generalized Morse wavelets belong to the family of analytic wavelets, and their Fourier transform is strictly positive along the real axis. CWT is particularly useful for analyzing signals with time-varying frequency and amplitude, as well as localized discontinuities. The resulting CWT produces RGB scalograms, which provide time-frequency spectra.

The dominant frequencies and corresponding scales extracted from these RGB scalograms are utilized to train and validate a signal classifier based on a Neural Network. These scalograms serve as input to the deep learning network, enabling the training and characterization of two distinct SCP classes: (i) UD and (ii) DSt.

Figure 3 illustrates the schematic representation of the SHM strategy, which employs a CNN-based deep learning approach for the automatic assessment of breathing debonds in SCPs. The training, validation, and testing processes of the designed CNN architecture are explained in detail below.

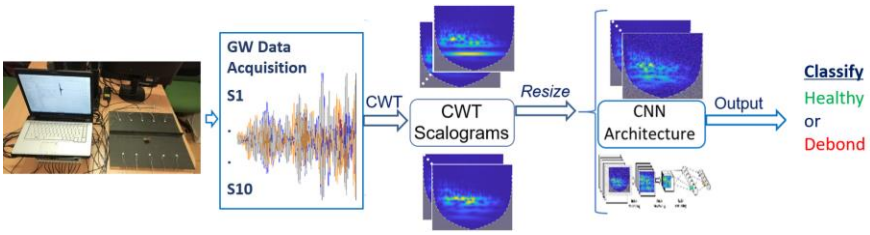

Figure 3. Deep learning based SHM strategy for healthy/debond SCP classification.

Figure 4 displays a block diagram illustrating the architecture of the designed CNN, which consists of six different layers. In this problem, each layer of the CNN performs specific functions, and a concise overview is provided here. For a more comprehensive understanding, refer to the detailed description in [15].

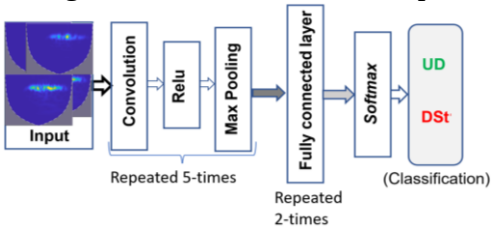

Figure 4. Designed architecture of the CNN for structural classification.

In the CNN algorithm, the input scalograms are first converted into RGB pixels and then fed into the network. In the present problem, each of the Red, Green, and Blue channels (i.e., RGB) has a dimension of [292×219 pixels]. Separate convolution kernels are assigned to each pixel matrix, and a bias is introduced after the convolution process. The outputs obtained from these three channels are combined to generate the output for this particular layer. To prevent any loss of information in subsequent layers, zero padding is applied after the convolution. The values of the bias and convolution kernel weights are updated using back-propagation.

RESULTS AND DISCUSSION

Experimental GW signals are collected for various cases. In Figure 5, representative GW signals obtained from the undamaged and damaged cases are displayed. It is observed that the GWs propagating through the SCP at 150 kHz exhibit multiple GW modes.

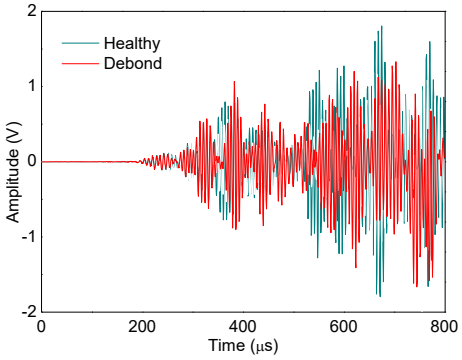

Figure 5. Typical GW signals correspond to the healthy (UD) and debond (DSt) cases.

The frequency-response analysis of the undamaged and debond-affected signals is presented in Figure 6, indicating the presence of higher harmonics resulting from the breathing phenomenon in the debond region. Notably, the second harmonic (HH1) is prominently observed in all debond cases.

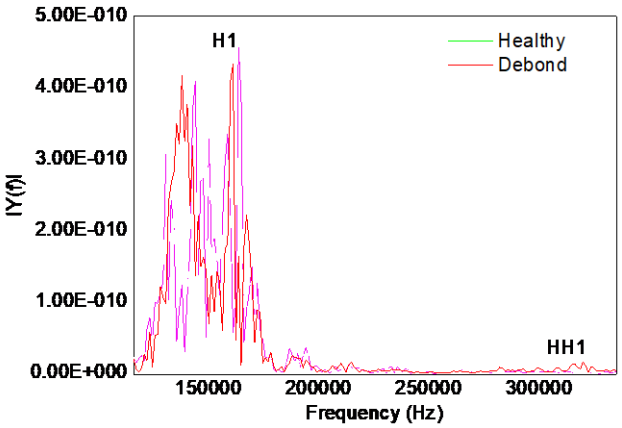

Figure 6. Healthy and breathing-debond informed raw GW signals in the frequency domain.

For the debond cases (DSt) and various actuator positions for the healthy cases (UD), experimental ultrasonic signals in the time domain are recorded from 10 PZT sensors. The GW dataset comprises two main classes, namely UD and DSt. In each case, the GW signals are captured from the 10 PZT sensors. These original time-domain signals, with a fixed window size of 800 microseconds, are then transformed into time-frequency CWT scalograms, as illustrated in Figure 7. The dimensions of each RGB scalogram image are determined to be [840×630×3] (length×width×channels) pixels.

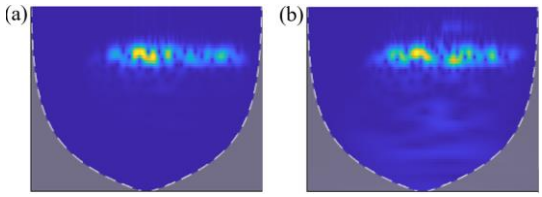

Figure 7. Reduced CWT scalograms of the recorded GW signals corresponding to (a) UD and (b) Dst.

The scalogram sizes (in pixels) were reduced to [292×219×3] to reduce computational costs. Additionally, 0-mean Gaussian noise ranging from 10% to 30% was randomly selected and added to the resized CWT scalograms for image augmentation, as illustrated in Figure 3. Gaussian noise follows a normal distribution, and for image augmentation, a random Gaussian function is added to introduce this noise. The zero mean value of the noise ensures that the positive and negative noise cancel each other out in the system, resulting in no net disturbance. A total of 3000 scalograms were obtained, of which 80% (i.e., 2400 scalograms) were used for training, 10% (i.e., 300 scalograms) for validation, and the remaining 10% (i.e., 300 scalograms) for testing the trained network. The deep learning network, described in Section 4, was trained, validated, and tested using datasets consisting of resized scalogram images corresponding to the UD and DSt classes. A 10-fold training/validation/test process was conducted to ensure the stable performance of the deep learning network. The 3000

images belonging to the UD and DSt classes were divided into 10 parts, with 300 images in each part. During training, Stage 1 used part-1 for testing and parts 2 to 10 for training/validation. Similarly, in Stage 2, part-1 was used for testing, and parts 3 to 10 were used for training/validation. This process was repeated for Stages 3 to 10 to improve confidence in the training progress. The validation accuracy and loss curves exhibited some oscillations during the early epochs due to the limited number of images per batch. After each batch passed through CNN, updated weight values were applied proportionally to all classes to prevent overfitting. To train the network, 10 epochs with 31 iterations per epoch were considered. Figure 8 illustrates a typical training and validation result, showing the validation accuracy and loss. The 10-fold training and validation results yielded an average accuracy of 97.4%.

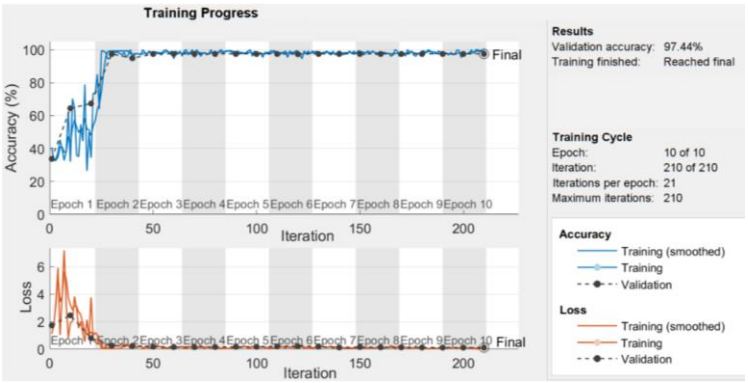

Figure 8. Training-validation plot represents the loss and accuracy.

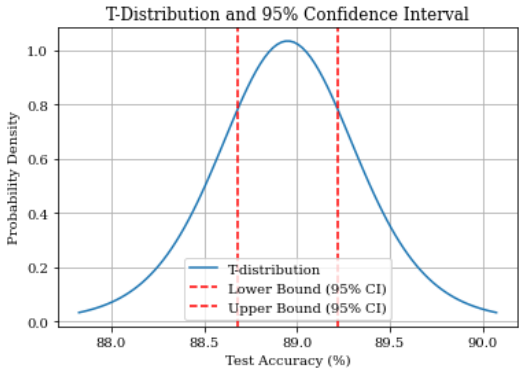

Figure 9. T -distribution of the 10-fold test performance shows the 95% CI of the trained SHM model.

The deep learning model was trained using the GW scalogram dataset, and its performance was evaluated using actual experimental data that was not included in the training process. The high accuracy achieved in the test results validates the potential of the proposed deep learning-based SHM model. The 10-fold av. test performance for healthy and debond classes are found to be 86.4% and 91.5%, respectively, whereas, the overall 88.95% average accuracy was obtained from the 10-fold test evaluation. Further, a T distribution plot in Figure 9 is obtained for the 10-fold test accuracy: [83.7, 83.8, 84, 84.3, 83.7, 84, 84.2, 83.8, 84, 84.3]%, sample Size: 10, mean: 88.95, standard deviation: 0.374907395973402, degrees of freedom: 9, and Confidence Interval (CI): [88.68180740519773, 89.21819259480228].

CONCLUSIONS

The research demonstrates the potential of this approach in accurately classifying breathing-debond regions in various bonded stiffened composite structures. By incorporating essential signal features through filtering and transformation, this monitoring strategy lays the groundwork for an automated system. The proposed methodology can be further explored for assessing a wide range of damages by leveraging acoustic fingerprints captured by the sensory network. The trained model can be deployed for real-time or online identification of damages in operational complex lightweight structures. In the specific study conditions, where SCP geometry and loading are considered, the registered GW signals exhibit a distinct HH1 signature indicative of breathing-debond. No other higher harmonics or sub-harmonics are observed. The test confusion charts of the trained deep learning network demonstrate the effectiveness of the SHM strategy in accurately classifying the two primary SCP classes: healthy and debond, using experimental untrained datasets with high precision.

REFERENCES

1. Matthews, F.L., and Rawlings, R.D. Composite Materials: Engineering and Science. Elsevier, 1999.
2. Shroff, S., Acar, E., and Kassapoglou, C. "Design, analysis, fabrication, and testing of composite grid-stiffened panels for aircraft structures." Thin-Walled Structures, vol. 119, 2017, pp. 235-246.
3. Zheng, K., Li, Z., Ma, Z., Chen, J., Zhou, J., and Su, X. "Damage detection method based on Lamb waves for stiffened composite panels." Composite Structures, vol. 225, 2019, article 111137.
4. Li, Z., Zhou, L., Lei, H., and Pei, Y. "Microwave near-field and far-field imaging of composite plate with hat stiffeners." Composites Part B: Engineering, vol. 161, 2019, pp. 87-95.
5. Sikdar, S., Fiborek, P., Kudela, P., Banerjee, S., & Ostachowicz, W. "Effects of debonding on Lamb wave propagation in a bonded composite structure under variable temperature conditions." Smart Materials and Structures, vol. 28, no. 1, 2018, p. 015021.
6. Kundu, T. "Fundamentals and Applications of Nonlinear Ultrasonic Nondestructive Evaluation." Ultrasonic and Electromagnetic NDE for Structure and Material Characterization, edited by T. Kundu, CRC Press, 2016, pp. 410-471.
7. De Luca, A., et al. "Numerical Investigation on Guided Waves Dispersion and Scattering Phenomena in Stiffened Panels." Materials, vol. 15, no. 1, 2021, p. 74.
8. Kundu, T. (Ed.). "Nonlinear ultrasonic and vibro-acoustical techniques for nondestructive evaluation." Springer, 2018.
9. Sikdar, S., Van Paepegem, W., Ostachowicz, W., & Kersemans, M. "Nonlinear elastic wave propagation and breathing-debond identification in a smart composite structure." Composites Part B: Engineering, vol. 200, 2020, p. 108304.
10. Yang, Y., Ng, C. T., Kotousov, A., Sohn, H., & Lim, H. J. "Second harmonic generation at fatigue cracks by low-frequency Lamb waves: Experimental and numerical studies." Mechanical Systems and Signal Processing, vol. 99, 2018, pp. 760-773.
11. He, Y., Xiao, Y., Su, Z., Pan, Y., & Zhang, Z. "Contact acoustic nonlinearity effect on the vibro-acoustic modulation of delaminated composite structures." Mechanical Systems and Signal Processing, vol. 163, 2022, article number 108161.
12. Naresh, M., Sikdar, S., & Pal, J. "Vibration data-driven machine learning architecture for structural health monitoring of steel frame structures." Strain, vol. 2023, article number e12439.
13. Sikdar, S., & Pal, J. "Bag of visual words based machine learning framework for disbond characterisation in composite sandwich structures using guided waves." Smart Materials and Structures, vol. 30, no. 7, 2021, article number 075016.
14. Pal, J., Sikdar, S., & Banerjee, S. "A deep-learning approach for health monitoring of a steel frame structure with bolted connections." Structural Control and Health Monitoring, vol. 29, no. 2, 2022, article number e2873.
15. Yamashita, R., Nishio, M., Do, R. K., & Togashi, K. "Convolutional neural networks: an overview and application in radiology." Insights into Imaging, vol. 9, no. 4, 2018, pp. 611-629.